Journal of Biomaterials and Nanobiotechnology, 2024, 15, 25-37
https://www.scirp.org/journal/jbnb
ISSN Online: 2158-7043
ISSN Print: 2158-7027

Calculating the Crystallite Size of *Microsorum scolopendria* AgCl Nanoparticles and Their Biological Activities

Christian Nanga Chick[1*], Mohammed Mahdaly[1], Phillippe Belle Ebanda Kedi[2,3], Kiuchi Sonoko[4], Francois Eya'ane Meva[2,5]

[1]Department of Materials and Life Sciences, Faculty of Science and Technology, Sophia University, Tokyo, Japan
[2]Laboratory of Innovative Nanostructured Material (NANO: C), Faculty of Medicine and Pharmaceutical Sciences, The University of Douala, Douala, Cameroon
[3]Nanosciences African Network, iThemba LABS-National Research Foundation, Cape Town, South Africa
[4]Department of Studies in Human Life Sciences, Otsuma Women's University, Tokyo, Japan
[5]Institute for Inorganic Chemistry and Structural Chemistry, Heinrich-Heine-University Düsseldorf, Düsseldorf, Germany
Email: *chicknanga0@gmail.com

How to cite this paper: Chick, C.N., Mahdaly, M., Kedi, P.B.E., Sonoko, K. and Meva, F.E. (2024) Calculating the Crystallite Size of *Microsorum scolopendria* AgCl Nanoparticles and Their Biological Activities. *Journal of Biomaterials and Nanobiotechnology*, **15**, 25-37.
https://doi.org/10.4236/jbnb.2024.152002

Received: April 20, 2024
Accepted: April 27, 2024
Published: April 30, 2024

Abstract

In this work, AgCl nanoparticles were synthesized from *Microsorum scolopendria* (MS) aqueous extract and $AgNO_3$ solution. Preliminary confirmation was a color change from a light brown to a dark-colored solution and a UV-Vis spectra surface plasmon resonance peak at 427 nm. Measured vibrational frequencies at 1713 cm^{-1} and 1030 cm^{-1} for C-O stretching of carboxylic acid or aliphatic ketone, and 1547 cm^{-1} for possibly N-O stretching of nitro compounds by Infrared (FTIR) analysis explain the possible biomaterial electronegative species or functional groups responsible for the reduction of Ag (+1) to Ag (0) for the formation of MS-AgCl nanoparticles. XRD analysis studies revealed that these particles contained face-centered cubic crystallites of metallic AgCl of 100 % with an average calculated crystallite size range of 30.34 nm (*SD* = 5.10 nm) by Scherrer's equation and a calculated crystallite size of 66.04 nm with a lattice strain of 0.00175 nm by Williamson Hall equation. The measured albumin denaturing activity of MS-AgCl nanoparticles gave an IC_{50} value of 26.70 μg/mL and 1.35 μg/mL for the positive control diclofenac. Additionally, the measured ability of phosphomolybdate complex formation, the antioxidant IC_{50} value of MS-AgCl nanoparticles was 35.29 μg/mL, and positive control ascorbic acid was 13.91 μg/mL. In all, using MS fern frond aqueous extracts, this preliminary work confirms MS-AgCl nanoparticles as potential therapeutic agents for oxidative stress, inflammatory problems, and related diseases.

Keywords

Microsorum scolopendria, SNPs, IR, UV-Vis, Antioxidant

1. Introduction

The characterizations of nanometric particles are vital for their accurate and reliable definition as they are synthesized from various biological, mechanical, or chemical routes. The properties of nanoparticles, such as their large surface area-to-volume ratio and their size-dependent applicability of functions, make characterization a necessity for the understanding of their uses at different molecular levels. Thus, without proper characterization of nanomaterials, their huge potential technological applications and academic research interests across several fields would encounter enormous difficulty. [1]

A few characterization tools are used to study a specific property of a material, while others are combined. Transmission electron microscopy, scanning electron microscopy, and atomic force microscopy provide information on the size, morphology, and crystal structure of nanomaterials, whereas superconducting quantum interference device, vibrating sample magnetometer, and ferromagnetic resonance are used for specialized magnetic nanomaterials. [2] [3] [4] For the structures, elemental composition, optical properties, and other physical properties of the nanomaterials, X-ray spectroscopy and scattering techniques are important. [5]

X-ray diffraction (XRD) analysis is one of the forefront characterization methods in the pharmaceutical industry, nanotechnology research, and manufacturing for a wide range of applications, generating critical data for users in many areas of drug discovery, development, and production. XRD quantitative methods determine the phase composition, lattice parameter, crystalline size, and degree of crystallinity of nanomaterials important for the plasmonic or catalytic properties of nanomaterials. [6] Some of the methods used for quantitative analysis are Scherrer's equation, Williamson Hall method, Warren-Averbach analysis, Rietveld refinement, and pseudo-Voigt function. [7] [8]

The fern *Microsorum scolopendria* (MS), commonly called the monarch fern belongs to the family of polypodiaceae. Very few reports exist for the fern MS and a recent phytochemical study demonstrated their rich phenolics and flavonoid contents such as protocatechic acid, 4-O-glucoside, cirsimaritin, and isoxanthohumol. [9] Phenolics or polyphenolics as well as flavonoids are widely used in food industries, cosmetics pharmaceutics due to their antioxidant, antimicrobial, and anti-inflammatory activities. [10] [11] Importantly, metal ions coordination interaction with phenolic hydroxyl group-containing bio-organic molecules in natural plants is exploited for the preparation of important nanoparticles for drug delivery, bio-imaging, surface modification, and disease treatment. [12]

This work focuses on the use of *Microsorum scolopendria* aqueous extract as a source of biomolecules such as polyphenols and flavonoids, and $AgNO_3$ as a source of metal ions. For the first time, AgCl nanoparticle synthesis using a green method was achieved with these components. The crystallite size and lattice strain of the nanoparticles were calculated using data from X-ray diffraction analysis. Furthermore, the ability of the nanoparticles to promote the formation of phosphomolybdate complex and inhibit egg albumin denaturation is explained, suggesting their potential pharmacological applications as an antioxidant and anti-inflammatory agent, respectively.

2. Ethical Considerations

All experiments were according to the approved protocol by the Institutional Ethical Committee of the University of Douala (Protocol approval number CEI-UDo/1399/04/2018/T).

3. Materials and Experimentation

Silver nitrate ($AgNO_3$) was purchased from Sigma Aldrich Co Ltd Germany, diclofenac from R. P. Normapur Prolabo® (Paris, France), centrifuge (Hettich D-7200 Tuttlingen, Germany), UV-Visible measurement with SPECORD S600 spectrometer operating at 1nm resolution, FT-IR with a Thermos Scientific Nicolet IS5 Model with the resolution of 0.4 cm^{-1}, powder X-ray diffraction (XRD) measurement using a Bruker D2 Phaser (CuKα wavelength of 1.540598 Å at 30 kV) by preparing a film of the SNPs powder on a flat low background silicon sample holder, and Origin Software version 9.6 (Northampton, MA, USA) for the calculation of full-width half maximum (FWHM) using XRD data.

The collection of the plant *Microsorum scolopendria* (Burm.f.) Copel (**Figure 1(A)**) was at Bonaberi (4˚06'19.3" N 9˚37'32.7" E), Littoral region, Cameroon. The verification and taxonomical coverage of the ferns were at the National Herbarium of Cameroon, Yaounde, and the pteridophytes were per the voucher specimen's herbarium number 18496 SRFCam. The ferns fresh frond was washed with running tap water and then distilled water. 10 grams of the fern was macerated with 100 mL of preheated distilled water (80˚C) and stirred for five minutes. The extracts were filtered and stored at 4˚C for further use.

The fern aqueous extracts mixed with 1 mM of $AgNO_3$ solution (volume ratio 1:5) were incubated in the dark at room temperature to minimize photoactivation of $AgNO_3$. [13] The incubated solution was visually monitored for color changes and UV-Vis spectroscopy measurement was also taken at the initial process of mixing and after 24 hrs. The solution color changed from a light to a dark brown color solution (c) after the addition of $AgNO_3$ solution (a) and the aqueous extract solution (b), as in **Figure 1(B)**.

Same as in other studies, this color change indicates the reduction of Ag (+) to Ag (0) with the plant biomaterials acting possibly as reducing agents, capping, and/or stabilizing agents as shown in **Figure 2**. [14] [15] [16]

(A)

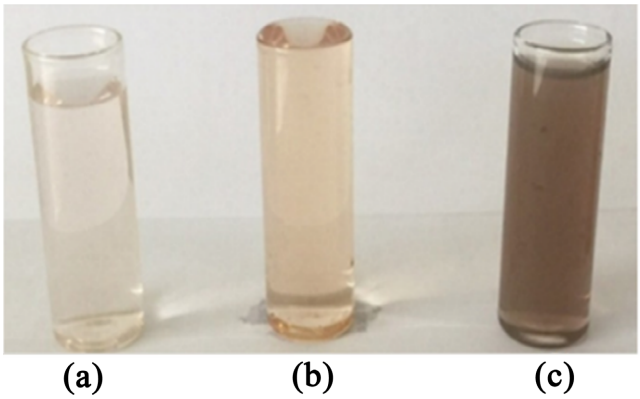

(B)

Figure 1. (A) *Microsorum scolopendria* (Burm.f.) Copel; (B) $AgNO_3$ solution (a), *M. scolopendria* (MS) aqueous extract (b), and MS-AgCl nanoparticles solution (c).

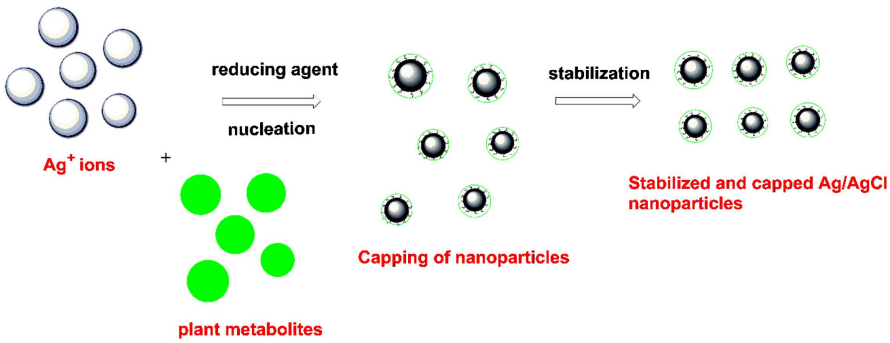

Figure 2. The reduction mechanism of Ag+ to Ag0 by plant biomaterials.

The UV-Vis measurement for the synthesized MS-AgCl nanoparticles demonstrates the formation of a surface plasmon resonance (SPR) peak, at about 427 nm for *Microsorum scolopendria* silver nanoparticles following 24 hrs of incubation (**Figure 3**).

The FTIR (infrared) measurement at wavenumber between 4000 to 500 cm^{-1} illustrated in **Figure 4** is taken for MS-AgCl nanoparticles. Absorption bands at 1713 cm^{-1} were for probably C-O stretching of carboxylic acid or aliphatic ke-

tone, at 1547 cm^{-1} was possibly for N-O stretching of nitro compounds, and several aromatic out-of-plane C-H and in-plane bending at the bands 1030 cm^{-1} could be for C-O stretching, 956 cm^{-1} and 805 cm^{-1} for probably C-H, C=C bending of alkene. [17] Thus, illustrating the functional groups of the biomaterials involved in either the reduction, capping, and/or stabilization of the formed AgCl-NPs.

The powder X-ray diffraction (XRD) pattern of MS-AgCl-NP was measured. The Rietveld refinement pattern graphics and the principal characteristic data are demonstrated in **Figures 5** and **Table 1**, respectively. The diffractogram data was compared with the standard powder diffraction cards of the Joint Committee of Powder Diffraction Standards (JCPDS) files number <31-1238> for AgCl. The cubic phase of AgCl of *M. scolopendria* at diffraction points 2θ values of 27.82˚, 32.24˚, 46.22˚, 54.81˚, 57.45˚, 67.39˚, 74.35˚, 76.72˚, and 85.66˚ were indexed to (111), (200), (220), (311), (222), (400), (331), (420), and (422) planes, respectively. The nanoparticle parameters such as the crystallite sizes (*D*) and/or lattice strain of the MS-AgClNPs were calculated using Scherrer's and Williamson Hall equations. [7] [8]

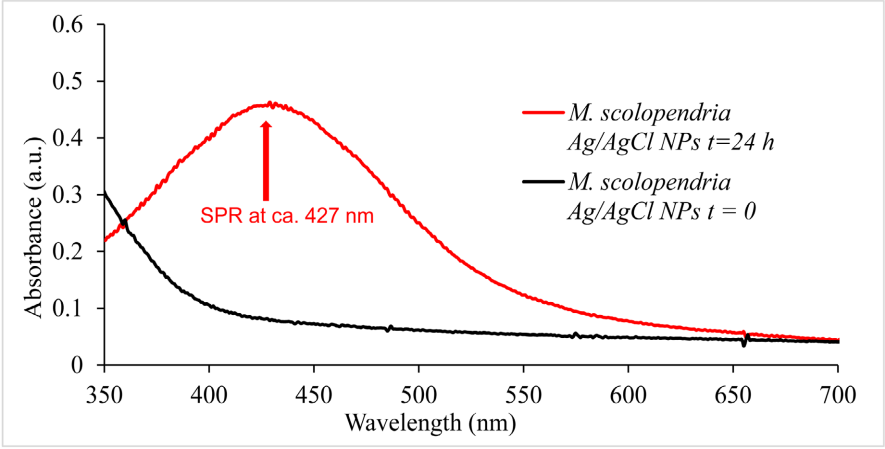

Figure 3. SPR peak for MS-AgCl nanoparticles after 24 hrs of incubation.

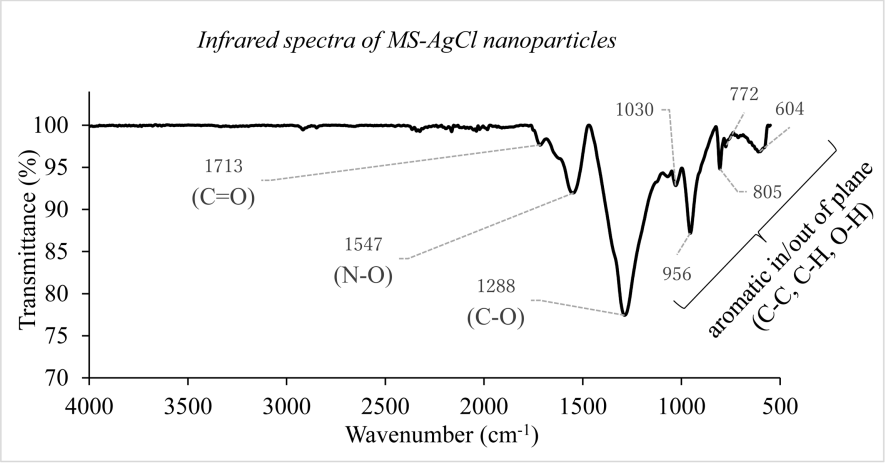

Figure 4. UV-Vis spectra of Ms.-Ag/AgCl NPs after incubation.

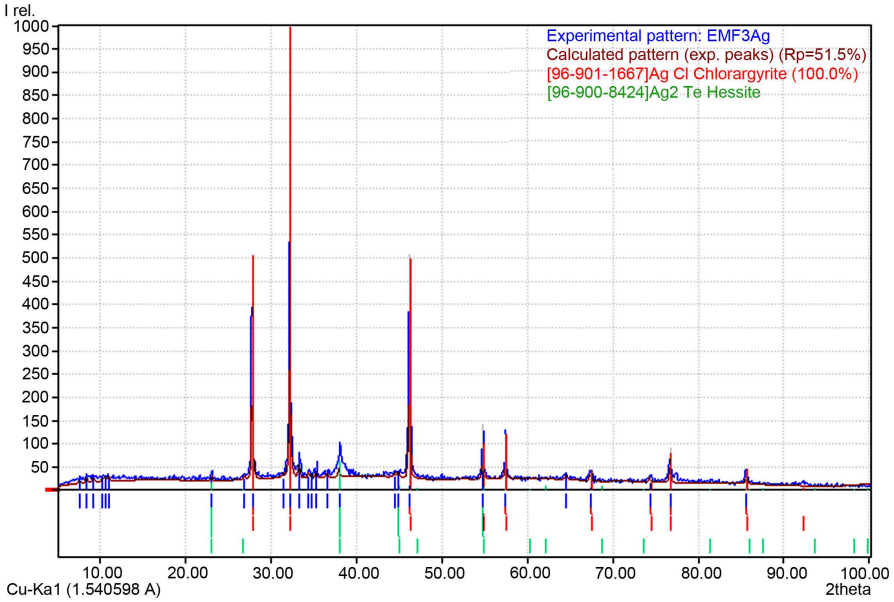

Figure 5. Rietveld X-ray diffractogram of MS-AgClNPs.

Table 1. MS-SNPs XRD principal characteristic data.

No.	Position [˚2Theta]	Peak height [cps]	d [nm]	Miller indices
1	27.82	485.6	0.32	111
2	32.24	1000.0	0.28	200
3	46.22	507.9	0.20	220
4	54.81	140.8	0.17	311
5	57.45	119.7	0.16	222
6	67.39	44.5	0.14	400
7	74.35	30.6	0.13	331
8	76.72	90.1	0.12	420
9	85.66	42.02	0.11	422

For the XRD broadening, using the intense peaks, the full width at half maximum (FWHM) obtained by Origin Software can be used to calculate the crystallite size and lattice strain of MS-AgClNPs. The observed X-ray peak has a broadening of β_0 and the broadening due to instrument effect is β_i, so the broadening of the peak due to crystallite size and lattice strain β_{hkl} is expressed as per Gaussian profile as: ($\beta_{hkl}^2 = \beta_0^2 - \beta_i^2$). [18] The Scherrer method considers only the crystallite size for the peak broadening as per the formula: $D = \frac{0.9\lambda}{\beta \cos\theta}$, where D is the crystallite size (nm), λ is the wavelength of the X-ray used for diffraction (0.1541 nm), and $\beta_{hkl} = \beta_{crystallite}$ is FWHM with peak broadening due to the crystallite independent of the lattice strain. [7] [8] [19] The calculation for the average crystallite size for MS-AgCl-NPs is illustrated in **Table 2**.

The Williamson Hall (W.H.) models rely on crystallite size and lattice strain-dependent broadening. [8] [19] From the formula: $\beta\cos\theta = 4\varepsilon\sin\theta + \frac{0.9\lambda}{D}$ where ε is the lattice strain. The linear equation $y = 0.007x + 0.0021$ obtained from the plot of $\beta_{hkl}\cos\theta$ against $\sin\theta$ (**Figure 6**), the values of the crystallite size and lattice strain are calculated as shown in **Table 3**.

The heat-induced egg albumin denaturation test for the anti-inflammatory study was applied. [14] [16] The percentage inhibition of albumin denaturation was proportional to the concentration of the MS-AgCl-NPs and the positive control (diclofenac). The latter was twenty times more potent as confirmed by their respective IC_{50} of 26.70 mg/mL and 1.35 µg/mL. The results were dose-dependent as shown in **Table 4**, and the values with $P < 0.05$ were considered significant.

Table 2. Scherrer crystallite size calculation data for MS-AgCl-NPs.

2θ	27.82	32.24	46.22	54.81	57.45		
β_{hkl} (rad.)	0.0041	0.0039	0.0054	0.0061	0.0060	**Average**	**SD**
D (nm)	34.92	37.30	27.68	25.44	26.36	**30.34**	**5.40**

*SD = Standard deviation.

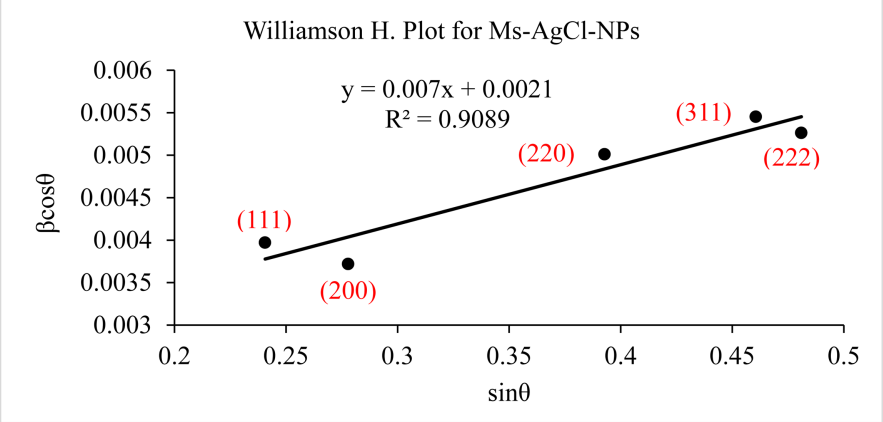

Figure 6. Williamson Hall (W.H.) plot for MS-AgCl-NPs.

Table 3. Crystallite size and lattice strain for MS-AgCl-NPs by Williamson H. equation.

2θ (degree)	27.82	32.24	46.22	54.81	57.45
θ (rad.)	0.2430	0.2816	0.4037	0.4787	0.5018
β (rad.)	0.0041	0.0039	0.0054	0.0061	0.0060
βcosθ	34.92	37.30	27.68	25.44	26.36
sinθ	0.0040	0.0037	0.0050	0.0055	0.0053
$\varepsilon = 0.00175$			$D = 66.04$ nm		

Table 4. Albumin denaturation assay for MS-AgCl-NPs.

Sample	Concentration (µg/mL)	% Inhibition (Mean ±*SD*)	IC_{50} (µg/mL)
Control	-	-	-
MS-AgCl-NPs	100	68 ± 0.8	26.70
	50	55 ± 1.2	
	25	48 ± 0.5	
	12.5	43 ± 1.9	
	6.25	32 ± 2.9	
Diclofenac	100	81 ± 1.5	1.35
	50	79 ± 1.0	
	25	77 ± 1.0	
	12.5	67 ± 1.04	
	6.25	60 ± 2.5	

*SD = Standard deviation; IC50 values are calculated as previously reported using Microsoft Excel. [14]

Table 5. Phosphomolybdenum assay for MS-AgCl-NPs.

Sample	Concentration (µg/mL)	% Inhibition	IC_{50} (µg/mL)
Control	-	-	-
MS-AgCl-NPs	100	92 ± 3.4	35.29
	50	76 ± 2.6	
	25	12 ± 0.5	
	12.5	06 ± 1.9	
	6.25	02 ± 1.3	
Ascorbic acid	100	85 ± 1.0	13.91
	50	80 ± 1.5	
	25	60 ± 1.3	
	12.5	40 ± 1.0	
	6.25	40 ± 2.6	

*SD = Standard deviation; IC50 values are calculated as previously reported using Microsoft Excel. [14]

The phosphomolybdenum reduction test measures the antioxidant abilities of compounds such as MS-AgCl-NPs and ascorbic acid (positive control) at concentrations of 100 mg/mL to 6.25 mg/mL to reduce Mo (VI) to Mo (V) resulting in

the formation of phosphomolybdenum complex. [16] For this assay, the prepared samples are heated at 95˚C, allowed to cool, and then measured with the UV-Vis spectrophotometer at 694 nm. The calculated IC50 values were 13.91 mg/mL for the positive control ascorbic acid and 35.29 mg/mL for MS-AgCl-NPs. These results were dose dependent as shown in **Table 5**, and the differences were significant ($p < 0.05$).

4. Discussion

The color change of the incubated MS-AgCl-NPs solution from a light to a dark brown colored solution confirms the formation of AgNPs with SPR peak at 427 nm after 24 hrs of incubation. As a merit to the multiple characterization methods of a nanomaterial, their morphology, surface chemistry, surface area, and disparity of nature are met. Thus, to exploit the surface chemistry of MS-AgNPs, infrared measurement showed vibrational frequencies at bands 1713 cm^{-1} and 1030 cm^{-1} for C-O stretching of carboxylic acid or aliphatic ketone, and 1547 cm^{-1} for possibly N-O stretching of nitro compounds. These electronegative species or functional groups are from the biomaterials responsible for the possible reduction, capping, or stabilization of the AgNPs.

XRD analysis helped to penetrate the crystalline core or phase of the MS-AgNPs for which 100 % AgCl peaks are observed. According to Scherrer's equation, the MS-AgCl-NPs average crystallite size of 30.34 nm is solely responsible for the peak broadening. From the Williamson-Hall equation, the crystallite size is 66.04 nm, and the lattice strain is 0.00175. The crystallite size using Scherrer's equation was smaller since the lattice strain is a non-dependent factor for the equation or for influencing the peak broadening. [20] The lattice strain is the measure of the distribution of the lattice constants arising from crystal imperfection (lattice dislocation), including vacancies, dislocations, and stacking faults. [21] The crystal structure, including defects and (surface) strain, is just as essential since it will directly affect the plasmonic or catalytic properties of a material. [22]

Metallic nanoparticles are among the numerous drug delivery systems used as a novel platform for various therapeutic purposes due to their unique properties and characteristics. Over the years nanoparticles have been widely used in many medical applications, such as biosensing, drug delivery, imaging, antimicrobial treatment, and reviewed strategies against viruses to fight future pandemics. Due to the particulate nature, morphology, and sizes, nanoparticle (NP)-based strategies present a powerful approach for their medical applications. AgNPs for instance can sustainably release Ag+ in and out of biological systems and can interact with proteins and enzymes. [23] [24]

Non-steroidal Anti-inflammatory Drugs (NSAIDs) such as diclofenac reduce and help prevent blood clots. They do so by blocking cyclooxygenases (COX) which are involved in the synthesis of prostaglandins which in turn are mediators. [25] AgNPs suppress the production of pro-inflammatory cytokines like interleu-

kin-12, and tumor necrosis factor-α and bring about the reduction in COX-2 gene expression which assists in achieving its anti-inflammatory potential. [26] Using MS leaves and root extracts indicated a selective inhibition of the COX-2 and COX-1 enzymes, with the root extracts having a slightly higher selectivity index than the leaves extract. [9] For the first time in this study, albumin denaturation assay for the AgNPs of MS is investigated giving an IC_{50} of 35.29 mg/mL which is about one-third as potent as the standard compound ascorbic acid. At a maximum tested concentration of 100 mg/mL, the highest inhibition of MS-AgNPs was observed confirming their possible anti-inflammatory potential at higher concentrations comparable to the standard compound.

Investigation of AgNPs' scavenging strength of reactive oxygen species and their possible reduction of cellular molecules was confirmed with the phosphomolybdate reduction test. In this test, the IC50 of MS-AgCl-NPs shows a potency three times comparable to the positive control compound, ascorbic acid. Recent studies using the reversed-phase high-performance liquid chromatography (RP-HPLC) mass spectrometer have shown that MS roots and leaves ethyl acetate extract are composed of high flavonoids and polyphenols with good DPPH (1,1-diphenyl-2-picrylhydrazyl) and ORAC (oxygen radical absorbance capacity) activities. The root extracts have higher activity compared to the leaves extracts. [9] At the nanoscale size, nanoparticles exhibit significantly different characteristics and improved bioactivity compared to their bulk counterpart. [27] Thus MS-AgCl-NPs are better potential antioxidant molecules.

5. Conclusion

Overall, AgNPs were synthesized from the aqueous extract of *M. scolopendria*. They consist of biomaterials that plausibly act as reducing, capping, or stabilizing agents. The formed nanoparticles are spherical in shape, which was confirmed by UV-Vis spectroscopy and XRD analytical methods. Their antioxidant and anti-inflammatory activities were also confirmed, showing their effectiveness against free radicals or oxidizing agents, as well as their potential as anti-inflammatory agents. Therefore, this work justifies the use of *M. scolopendria* AgCl-NPs as a novel, effective, and safe approach for designing future antioxidant and anti-inflammatory medications for potential pharmaceutical use. However, further investigation is required for alternative in vitro, in vivo, toxicity, and pharmacological studies.

Conflicts of Interest

The authors declare no conflicts of interest.

References

[1] Thanh, N.T.K., Maclean, N. and Mahiddine, S. (2014) Mechanisms of Nucleation and Growth of Nanoparticles in Solution. *Chemical Reviews*, **114**, 7610-7630. https://doi.org/10.1021/cr400544s

[2] Kedi, P.B.E., Nanga, C.C., Gbambie, A.P., *et al*. (2020) Biosynthesis of Silver Nanoparticles from *Microsorum punctatum* (L.) Copel Fronds Extract and an *in-vitro* Anti-Inflammation Study. *Journal of Nanotechnology Research*, **2**, 25-41. https://doi.org/10.26502/jnr.2688-85210014

[3] Driskell, J.D., Larrick, C.G. and Trunell, C. (2014) Effect of Hydration on Plasmonic Coupling of Bioconjugated Gold Nanoparticles Immobilized on a Gold Film Probed by Surface-Enhanced Raman Spectroscopy. *Langmuir*, **30**, 6309-6313. https://doi.org/10.1021/la500640q

[4] Sandler, S.E., Fellows, B. and Mefford, O.T. (2019) Best Practices for Characterization of Magnetic Nanoparticles for Biomedical Applications. *Analytical Chemistry*, **91**, 14159-14169. https://doi.org/10.1021/acs.analchem.9b03518

[5] Sanchez-Cano, C., Alvarez-Puebla, R.A., Abendroth, J.M., Beck, T., Blick, R., Cao, Y., Caruso, F., Chakraborty, I., Chapman, H.N., Chen, C., Cohen, B.E., Conceição, A.L., Cormode, D.P., Cui, D., Dawson, K.A., Falkenberg, G., Fan, C., Feliu, N., Gao, M., Parak, W.J., *et al*. (2021) X-Ray-Based Techniques to Study the Nano-Bio Interface. *ACS Nano*, **15**, 3754-3807. https://doi.org/10.1021/acsnano.0c09563

[6] Holder, C.F. and Schaak, R.E. (2019) Tutorial on Powder X-Ray Diffraction for Characterizing Nanoscale Materials. *ACS Nano*, **13**, 7359-7365. https://doi.org/10.1021/acsnano.9b05157

[7] Bushkova, V.S., Mudry, S.I., Yaremiy, I.P. and Kravets, V.I. (2016) X-Ray Analysis of Nickel-Cobalt Ferrite Nanoparticles by Using Debyeв-Scherrer, Williamsonв-Hall and SSP Methods. *Journal of Physical Studies*, **20**, Article 1702. https://doi.org/10.30970/jps.20.1702

[8] Mustapha, S., Ndamitso, M.M., Abdulkareem, A.S., Tijani, J.O., Shuaib, D.T., Mohammed, A.K. and Sumaila, A. (2019) Comparative Study of Crystallite Size Using Williamson-Hall and Debye-Scherrer Plots for ZnO Nanoparticles. *Advances in Natural Sciences*: *Nanoscience and Nanotechnology*, **10**, Article 045013. https://doi.org/10.1088/2043-6254/ab52f7

[9] Balada, C., Díaz, V., Castro, M., Echeverría-Bugueño, M., Marchant, M.J. and Guzmán, L. (2022) Chemistry and Bioactivity of *Microsorum scolopendria* (Polypodiaceae): Antioxidant Effects on an Epithelial Damage Model. *Molecules*, **27**, Article 5467. https://doi.org/10.3390/molecules27175467

[10] Shahidi, F. and Ambigaipalan, P. (2015) Phenolics and Polyphenolics in Foods, Beverages and Spices: Antioxidant Activity and Health Effects—A Review. *Journal of Functional Foods*, **18**, 820-897. https://doi.org/10.1016/j.jff.2015.06.018

[11] Hu, M., Wu, B. and Liu, Z. (2017) Bioavailability of Polyphenols and Flavonoids in the Era of Precision Medicine. *Molecular Pharmaceutics*, **14**, 2861-2863. https://doi.org/10.1021/acs.molpharmaceut.7b00545

[12] Wu, D., Zhou, J., Creyer, M.N., Yim, W., Chen, Z., Messersmith, P.B. and Jokerst, J.V. (2021) Phenolic-Enabled Nanotechnology: Versatile Particle Engineering for Biomedicine. *Chemical Society Reviews*, **50**, 4432-4483. https://doi.org/10.1039/d0cs00908c

[13] Bogatyrov, V.M., Gun'ko, V.M., Galaburda, M.V., Oranska, O.I., Petryk, I.S., Tsyganenko, K.S., Savchuk, Y.I., Chobotarov, A.Y., Rudenchyk, T.V., Rozhnova, R.A. and Galatenko, N.A. (2019) The Effect of Photoactivated Transformations of Ag^{+} and Ag^{0} in Silica Fillers on Their Biocidal Activity. *Research on Chemical Intermediates*, **45**, 3985-4001. https://doi.org/10.1007/s11164-019-03885-2

[14] Chick, C.N., Misawa-Suzuki, T., Suzuki, Y. and Usuki, T. (2020) Preparation and Antioxidant Study of Silver Nanoparticles of *Microsorum pteropus* Methanol Extract. *Bioorganic & Medicinal Chemistry Letters*, **30**, Article 127526.

https://doi.org/10.1016/j.bmcl.2020.127526

[15] Luhata, L.P., Chick, C.N., Mori, N., Tanaka, K., Uchida, H., Hayashita, T. and Usuki, T. (2022) Synthesis and Antioxidant Activity of Silver Nanoparticles Using the *Odontonema strictum* Leaf Extract. *Molecules*, **27**, Article 3210. https://doi.org/10.3390/molecules27103210

[16] Meva, F.E.A., Mbeng, J.O.A., Ebongue, C.O., *et al*. (2019) *Stachytarpheta cayennensis* Aqueous Extract, a New Bioreactor towards Silver Nanoparticles for Biomedical Applications. *Journal of Biomaterials and Nanobiotechnology*, **10**, 102-119. https://doi.org/10.4236/jbnb.2019.102006

[17] Wongsa, P., Phatikulrungsun, P. and Prathumthong, S. (2022) FT-IR Characteristics, Phenolic Profiles and Inhibitory Potential against Digestive Enzymes of 25 Herbal Infusions. *Scientific Reports*, **12**, Article No. 6631. https://doi.org/10.1038/s41598-022-10669-z

[18] Delhez, R., de Keijser, T.H. and Mittemeijer, E.J. (1982) Determination of Crystallite Size and Lattice Distortions through X-Ray Diffraction Line Profile Analysis. *Fresenius' Zeitschrift für Analytische Chemie*, **312**, 1-16. https://doi.org/10.1007/bf00482725

[19] Rabiei, M., Palevicius, A., Monshi, A., Nasiri, S., Vilkauskas, A. and Janusas, G. (2020) Comparing Methods for Calculating Nano Crystal Size of Natural Hydroxyapatite Using X-Ray Diffraction. *Nanomaterials*, **10**, Article 1627. https://doi.org/10.3390/nano10091627

[20] Kurian, M. and Kunjachan, C. (2014) Investigation of Size Dependency on Lattice Strain of Nanoceria Particles Synthesised by Wet Chemical Methods. *International Nano Letters*, **4**, 73-80. https://doi.org/10.1007/s40089-014-0122-7

[21] Nath, D., Singh, F. and Das, R. (2019) X-Ray Diffraction Analysis by Williamson-Hall, Halder-Wagner and Size-Strain Plot Methods of Cdse Nanoparticles—A Comparative Study. *Materials Chemistry and Physics*, **239**, Article 122021. https://doi.org/10.1016/j.matchemphys.2019.122021

[22] Novo, C., Funston, A.M. and Mulvaney, P. (2008) Direct Observation of Chemical Reactions on Single Gold Nanocrystals Using Surface Plasmon Spectroscopy. *Nature Nanotechnology*, **3**, 598-602. https://doi.org/10.1038/nnano.2008.246

[23] Du, T., Zhang, J., Li, C., Song, T., Li, P., Liu, J., Du, X. and Wang, S. (2020) Gold/Silver Hybrid Nanoparticles with Enduring Inhibition of Coronavirus Multiplication through Multisite Mechanisms. *Bioconjugate Chemistry*, **31**, 2553-2563. https://doi.org/10.1021/acs.bioconjchem.0c00506

[24] Medhi, R., Srinoi, P., Ngo, N., Tran, H.-V. and Lee, T.R. (2020) Nanoparticle-Based Strategies to Combat COVID-19. *ACS Applied Nano Materials*, **3**, 8557-8580. https://doi.org/10.1021/acsanm.0c01978

[25] Ong, C.K.S., Lirk, P., Tan, C.H. and Seymour, R.A. (2007) An Evidence-Based Update on Nonsteroidal Anti-Inflammatory Drugs. *Clinical Medicine & Research*, **5**, 19-34. https://doi.org/10.3121/cmr.2007.698

[26] Kumawat, M., Madhyastha, H., Singh, M., Revaprasadu, N., Srinivas, S.P. and Daima, H.K. (2022) Double Functionalized Haemocompatible Silver Nanoparticles Control Cell Inflammatory Homeostasis. *PLOS ONE*, **17**, e0276296. https://doi.org/10.1371/journal.pone.0276296

[27] Dube, P., Meyer, S., Madiehe, A. and Meyer, M. (2020) Antibacterial Activity of Biogenic Silver and Gold Nanoparticles Synthesized from *Salvia africana-lutea* and *Sutherlandia frutescens*. *Nanotechnology*, **31**, Article 505607. https://doi.org/10.1088/1361-6528/abb6a8

Abbreviations

MS-AgCl-NPs (*Microsorum scolopendria* silver chloride nanoparticles);
SPR (surface plasmon resonance);
XRD (X-ray diffraction);
UV-Vis (ultraviolet-visible) spectroscopy;
FWHM (full-width half maximum).